HHS Public Access

Author manuscript

J Cell Biochem. Author manuscript; available in PMC 2018 August 01.

Published in final edited form as:

J Cell Biochem. 2017 August ; 118(8): 2395–2408. doi:10.1002/jcb.25902.

Sodium butyrate protects against high fat diet-induced cardiac dysfunction and metabolic disorders in type II diabetic mice

Ling Zhang[1,3], **Jianfeng Du**[1], **Naohiro Yano**[2], **Hao Wang**[1], **Yu Tina Zhao**[1], **Dubielecka-Szczerba Patricia**[4], **Shougang Zhuang**[4], **Eugene Y Chin**[5], **Gangjian Qin**[6], and **Ting C Zhao**[1,*]

[1]Department of Surgery, Boston University School of Medicine, Roger Williams Medical Center, Providence, RI

[2]Women and Infants Hospital, Brown University, Providence, RI

[3]Department of Emergency Medicine, Rhode Island Hospital, Shanghai, China

[4]Department of Medicine, Rhode Island Hospital, Shanghai, China

[5]Key Laboratory of Stem Cell Biology, Institutes of Health Sciences, Shanghai Institutes for Biological Sciences, Chinese Academy of Sciences, Shanghai, China

[6]Feinberg Cardiovascular Research Institute, Northwestern University Feinberg School of Medicine, Chicago

Abstract

Histone deacetylases are recently identified to act as key regulators for cardiac pathophysiology and metabolic disorders. However, the function of histone deacetylase (HDAC) in controlling cardiac performance in type II diabetes and obesity remains unknown. Here we determine whether HDAC inhibition attenuates high fat diet (HFD)-induced cardiac dysfunction and improves metabolic features. Adult mice were fed with either HFD or standard chow food for 24 weeks. Starting at 12 weeks, mice were divided into four groups randomly, in which sodium butyrate (1%), a potent HDAC inhibitor, was provided to chow and HFD-fed mice in drinking water, respectively. Glucose intolerance, metabolic parameters, cardiac function, and remodeling were assessed. Histological analysis and cellular signaling were examined at 24 weeks following euthanization of mice. HFD-fed mice demonstrated myocardial dysfunction and profound interstitial fibrosis, which were attenuated by HDAC inhibition. HFD-induced metabolic syndrome features insulin resistance, obesity, hyperinsulinemia, hyperglycemia, lipid accumulations, and cardiac hypertrophy, these effects were prevented by HDAC inhibition. Furthermore, HDAC inhibition attenuated myocyte apoptosis, reduced production of reactive oxygen species, and increased angiogenesis in the HFD-fed myocardium. Notably, HFD induced decreases in MKK3, p38, p38 regulated/activated protein kinase (PRAK) and Akt-1, but not p44/42 phosphorylation, which were prevented by HDAC inhibition. These results suggest that HDAC inhibition plays a critical role to preserve cardiac performance and mitigate metabolic disorders in obesity and diabetes, which is associated with MKK3/p38/PRAK pathway. The study holds promise in

*Corresponding Author: Ting C Zhao, MD, Associate Professor, Department of Surgery, Boston University Medical School, Roger William Medical Center, 50 Maude Street, Providence, RI 02908, tzhao@bu.edu, Fax: 401-456-2507, Tel: 401-456-8266.

Disclosure: none.

developing a new therapeutic strategy in the treatment of type II diabetic-induced heart failure and metabolic disorders.

Keywords

histone deacetylase; diabetes; cardiovascular disease; obesity; cardiac function; metabolic syndrome

INTRODUCTION

High fat diet and eventual obesity predispose an individual to the development of a number of morbidities such as heart disease, hepatic disease, hypertension, diabetes mellitus, and dyslipidemia (Cook S et al., 2004; Kang JS et al., 2011;, Olsson B et al., 2015; Odermatt A et al., 2011; Shulman GI, 2014). Cardiovascular disease is the main cause of deaths in the diabetic population, which leads to a recent conception that diabetes is also regarded as cardiovascular disease (AHA, 2015). Although there are increasing efforts to treat diabetes and heart failure in diabetic patients, optimal treatment of cardiac dysfunction in diabetes and metabolic disturbance have not been specifically established. The pursuit for novel protective approaches that are effective for cardiac diseases has been brought to the limelight in recent years (Lamounier-Zepter V et al., 2009; Relling DP et al., 2006; Ren J et al., 2010).

Very recently, histone deacetylases and histone acetyltransferases are among the most important components in the modulation of pathological conditions in both diabetes and heart failure (Khan S & Jena G, 2015; Olson EN et al., 2006). Histone acetyltransferase (HAT) and histone deacetylase (HDAC) have emerged as crucial factors in the developing process of cardiac disorders with diverse etiologies (Kurdi M & Booz GW. 2011; Sun H et al., 2010). Recent evidence indicates that inhibition of HDAC ameliorates metabolic dysfunction, enhances energy consumption, improves insulin sensitivity, and evokes remarkably protective effects in the settings of pressure overload and ischemia/reperfusion (Du et al, 2015; Galmozzi A et al., 2013; Wang J et al., 2015, Ye J. 2013; Zhang L et al., 2012). The most exciting study reveals the novel potentiality that HDAC inhibitors could serve as a new target to treat diabetic disorders and insulin resistance (Newman JC & Verdin E, 2014). HDAC inhibitor therapy emerges as a novel means of arresting the untoward consequences of pathological cardiac stress, thus bringing clinical benefits to patients with heart failure. The recent observations from our lab indicate that HDAC inhibition with sodium butyrate suppresses cardiac dysfunction in type I diabetes (Chen Y et al., 2015). However, it remains unknown whether HDAC inhibition could preserve cardiac performance and mitigate the metabolic disturbance in high fat diet-induced obesity. The present study was undertaken to clarify whether HDAC inhibition could protect against myocardial dysfunction and metabolic disorders in type 2 diabetes. For this purpose, we employed the HFD mouse model for obesity to define the functional role of HDAC inhibition in improving cardiac dysfunction, remodeling, and metabolic disturbance, as well as its cellular signaling. The results of this study provide the first evidence that HDAC inhibition generates protective effects through preserving cardiac function and mitigating metabolic dysfunction in diabetic and obesity, which is related to the activation of p38 and PRAK pathways.

RESEARCH DESIGN AND METHODS

Animals and Experimental Protocol

Four-week old CD-1 mice of both genders were purchased from Charles River Laboratories (Wilmington, MA). All mice were housed at Animal Care Facility of Roger Williams Medical Center in a temperature-controlled room (22°C) on a 12-h light-dark cycle. Mice were then randomly divided into two groups and were fed with either a high-fat diet (60% fat, 20% carbohydrate, 20% protein, Research Diets, New Brunswick, NJ), or standard chow (10% fat, 70% carbohydrate and 20% protein, New Brunswick, NJ) for 24 weeks. Starting from the twelfth week, mice were further divided into four groups: Mice provided with chow and regular drinking water (Chow); Mice provided with chow and 1% Sodium Butyrate in drinking water (Chow+Butyrate); Mice provided with HFD and regular drinking water (HFD); and Mice provided with HFD and 1% Sodium Butyrate in drinking water (HFD +Butyrate). Mice were sacrificed by the end of the twenty-fourth week and tissues were collected for subsequent experiments (Figure 1). All animal procedures were approved by the Institutional Animal Care and Use Committee and followed the National Institute of Health guidelines on the care and use of animals.

Metabolic measurement

Glucose tolerance tests (GTT) were determined. Mice were fasted for 4 hours, and then baseline glucose level were measured using an Accu-Chek Compact Plus glucometer (Roche Diagnostics, Indianapolis, IN) by using tail vein blood. Mice were subsequently injected with 1 mg/g glucose intraperitoneally. Serum glucose levels were measured at 15, 30, 60, 120 and 240 min following glucose injection. Total serum cholesterol and fasting glucose were measured with a CardioChek PA system (PTS Diagnostics, Indianapolis, IN) according to the manufacturer's instructions using tail vein blood. Plasma insulin levels were measured using a Mouse Insulin ELISA kit from ALPCO (Salem, NH) following the manufacturer's instructions. Insulin content was determined using a standard curve obtained from the standards provided by the kit. Serum and liver triglyceride levels were evaluated using a Triglyceride Colorimetric Assay Kit from Cayman Chemical (Ann Arbor, MI) according to the manufacturer's instructions. Tail vein blood samples from the sacrificed animals were used for the analysis of serum triglycerides. Liver lipid was extracted using the solution provided by an identical analysis kit. Triglyceride levels were calculated using the absorbance readings of samples and triglyceride standards.

Cardiac functional measurements

Echocardiography of mice was serially conducted using an Acuson Sequoia C512 system equipped with a 15L8 linear array transducer to access left ventricular (LV) function. Briefly, mice were anesthetized with 1.5% isoflurane mixed with oxygen via a nose cone, and then placed in supine position on a heating pad. After removal of hair, the precordial region was covered with pre-warmed ultrasound transmission gel (Aquasonic, Parker Laboratory, Fairfield, NJ). Short axis of LV were chosen to capture two-dimensional B-mode images and M-mode tracing at the level of the papillary muscles. The signal depth was set at 25mm. Three to six consecutive cardiac cycles were measured from M-mode tracings with

accompanying software. All measurements were performed by a single experienced operator blinded to the group assignments.

Immunohistochemistry

Paraffin-embedded tissues were analyzed to assess cell surface area in both hearts and muscles. Tissue sections were stained with Wheat germ agglutinin (WGA, FITC-conjugated) overnight at 4°C. For angiogenesis assessment, sections were then stained with CD31 (Anti-PECAM-1) (Millipore, Billerica, MA) overnight at 4°C. Signals were then visualized by incubating at room temperature for 1 hour with Goat anti-Rat secondary antibody, (Alexa Fluor® 555 conjugate, Life Technologies, Carlsbad, CA). 4,6-Diamidino-2-Phenylindole (DAPI) (Life Technologies, Carlsbad, CA) was used to identify nuclei. Confocal fluorescent microscopy was performed using a Carl Zeiss LSM 700 laser scanning microscope equipped with intuitive ZEN 2009 software. 5–10 randomly selected high-power fields were selected for quantifications using Image J software. (NIH, version 1.40g, http://rsb.info.nih.gov/ij/). To evaluate cardiac fibrosis, LV sections were stained with picrosirius red and collagen content was quantified in images taken under a microscope coupled to a computerized morphometry system (Olympus BX41). Interstitial collagen density was expressed as a percentage of myocardial area in each image. Measurement of lipid accumulations in muscle and heart was determined with oil red O for lipid deposition by standard methods according to the description with modifications (Annika Mehlem nature protocol). The density of lipid accumulation was measured from 10 randomized areas of three sections in each heart.

Terminal deoxynucleotidyltransferase (TdT) nick-end labeling (TUNEL) was performed using a TACS 2-TdT-DAB In Situ Apoptosis Detection Kit (Trevigen Inc., Gaithersburg, MD) according to the manufacturer's instructions. To verify that apoptosis occurred in the myocytes, immunohistochemical staining was carried out with α-sarcomeric actin antibody (monoclonal, 1:100 dilution, Sigma; St. Louis, MO) at 4°C overnight. For each section, the number of TUNEL-positive myocyte nuclei was counted in five randomly selected regions. The index of apoptosis was then determined (i.e., number of apoptotic myocytes ÷ total number of myocytes counted × 100).

Dihydroethidium (DHE) staining

Superoxide production in hearts was detected by dihydroethidium staining (Sigma-Aldrich, St. Louis, MO). Heart sections were incubated with 10 μmol/l DHE at room temperature for 15 min in a humidified chamber protected from light. Fluorescent images were obtained with a Carl Zeiss LSM 700 confocal microscope. The mean DHE fluorescence intensity of myocyte nuclei was calculated with Image J software described above. Approximately 150–200 nuclei were measured in each field, and three to five fields in each section were randomly selected in the heart.

Real time polymerase chain reaction (*PCR)*

Total RNA was extracted from different groups with Trizol reagent (Life Technologies, Grand Island, NY). cDNA was synthesized from 5 μg of total RNA. The reverse transcribed cDNA (5 μL) was amplified to a final volume of 50 μL by PCR under standard conditions.

Real-time PCR experiments were performed on a master cycler realplex4 (Eppendorf North America) system using qPCR Kit master mix. (Kapabiosystems, Boston, USA). Atrial natriuretic peptide (ANP): Forward: CAC AGA TCT GAT GGA TTT CAA GA; REV: CCT CAT CTT CTA CCG GCA TC. GAPDH was used as the internal control. Three hearts in each group were utilized to determine mRNA content.

Immunoblotting and antibodies

We prepared samples from the myocardium and performed immunoblotting analysis. Proteins (50 μg/lane) were separated by SDS-PAGE and then transferred onto a nitrocellulose membrane. The blots were incubated with their respective antibodies. Phosphorylation levels of kinases were evaluated by Western blotting as previously described (Zhang et al, 2012). Antibodies against HDAC 1, HDAC2, HDAC3, HDAC4, HDAC10, β-actin, phosphorylated and total, MKK3, p38, PRAK, Akt-1 and p44/42 were purchased from Cell Signaling Technologies. Poly monoclonal active-caspase-3 antibody was obtained from Abcam (Cambridge, MA). The results were visualized with Super Signal West Pico chemiluminescent substrate (Thermo Scientific) and analyzed with the UN-SCAN-IT gel software for Windows (Silk Scientific, Inc., Orem, UT, USA).

Measurements of HDAC activity

Myocardial HDAC activity was measured as described preciously in detail (Chen Y et al, 2015).

Statistical analysis

All measurements are expressed as mean±SEM. Difference among groups were analyzed by one-way analysis of variance (ANOVA), followed by post hoc Bonferroni correction. Statistical differences were considered significant with a value of $p<0.05$.

RESULTS

Sodium butyrate treatment attenuates HFD induced obesity and hypercholesterolemia

HFD was initiated at 6 week of age as was the standard chow. As shown in Figure 2A, after 24 weeks on HFD, the body weight was significantly increased in the HFD only group (41.21±0.68 g), as compared to the standard chow fed (32.60±0.76 g, $p<0.01$vs. Chow food) and Chow + Butyrate groups (33.73±1.04 g, $p<0.001$ vs. HFD). This phenotypic change in body weight in mice fed with HFD indicates the development of obesity (Figure 2A). However, the increase in the average body weights of mice fed with HFD was mitigated by treatment of mice with sodium butyrate as compared to HFD group (37.26±0.72g in HFD +butyrate group, $p<0.05$ vs. HFD). There is not a significant difference in the average body weight at the baseline among these groups. As shown in Figure 2B, HFD also induced a higher serum cholesterol in HFD group (173±11.16 mg/dl) as compared to Chow (114±9.65 mg/dl, $p<0.001$) and Chow+Butyrate groups (106.33±3.01 mg/dl, $p<0.001$vs HFD). Administration of sodium butyrate reduced total cholesterol to a normal level in HFD fed mice (109.6±2.66 mg/dl in HFD+butyrate group, $p<0.001$ vs. HFD).

Sodium butyrate treatment attenuates HFD induced glucose intolerance

As shown in Figures 2C and 2D, both groups fed with standard chow showed a normal glucose response in glucose tolerance tests, while HFD group displayed glucose intolerance as revealed by GTT and the calculated area under the curve (A.U.C.) (1.89±0.02 folds of chow). Sodium butyrate corrected the glucose intolerance in HFD-fed mice (1.37±0.04 folds of chow, $p<0.001$ vs. HFD). Hyperglycemia was manifested in HFD-fed animals, which was also associated with hyperinsulinemia (Figure 2 E and F). HDAC inhibition mitigated the magnitude of both hyperinsulinemia and hyperglycemia in HFD-fed mice. Likewise, fat triglycerides in liver and serum were increased in HFD-induced obesity mice (Figure 2 G and H), which were also suppressed by treatment of sodium butyrate.

Sodium butyrate treatment restores HFD induced Left Ventricular dysfunction

Echocardiographic parameters were accessed to evaluate LV function in tested mice. As shown in Figures 3A and 3B, mice fed with HFD exhibited cardiac dysfunction, as indicated by the dramatic reduction in shortening fraction and ejection fraction as compared with Control Chow and Chow +butyrate groups. Likewise, mice fed with HFD also had an increased left ventricular internal dimension (LVID) in both systolic and diastolic stages as compared with LVID of mice fed with chow food (Figures 3C, 3D and 3G). However, the cardiac dysfunction caused by the high fat diet was prevented by inhibition of HDACs. Wall thickness (LVPW) increased in HFD-fed mice, which was mitigated by HDAC inhibition (Figure 3 E, 3F and 3G). In addition, the suppression of cardiac dysfunction in terms of LVID;s, LVID;d, EF and FS in HFD was also prevented by sodium butyrate during the course of treatment (Table 1–4).

Sodium butyrate treatment attenuated HFD induced cardiac hypertrophy

The ratio of heart weight to tibia length (HW/TL) was assessed to evaluate hypertrophic response. Mice in HFD group demonstrated increased HW/TL and heart weight/body weight ratios (HW/BW) as compared to Chow and Chow+Butyrate groups (Figures 4A and 4B). Treatment of sodium butyrate significantly reduced the heart weight/tibia length ratio and heart weight/body weight ratio (Figures 4A and 4B). Wheat germ agglutinin staining was performed to assess the cross sectional cardiomyocyte size. The HFD led to an increase in cross-sectional cardiomyocyte size as compared with Chow groups (145.64±4.50 % of chow) (Figures 4C and 4D). However, the cross-sectional cardiomyocyte size was reduced in HFD-fed mice receiving sodium butyrate as compared with HFD-fed mice alone (118.06±3.49 % of chow) (Figures 4C and 4D). Consistent with this observation, hypertrophic genes and atrial natriuretic peptide (ANP) were up-regulated in HFD, which was also suppressed by HDAC inhibition (Figure 4 E). The collagen content was significantly increased in myocardium from mice fed with HFD as compared to chow and chow + sodium butyrate groups (Figures 4 F and G). However, as compared with HFD-treated wild type mice, sodium butyrate treatment resulted in a significant reduction of interstitial collagen as induced by the HFD.

Sodium butyrate treatment prevents HFD induced apoptosis in myocardium

TUNEL staining was performed to evaluate the anti-apoptotic effect of sodium butyrate. HFD increased the number of TUNEL-positive nuclei in mouse myocardium (0.03 % in chow group, and 0.26 % in HFD group, $p<0.001$), but HDAC inhibition significantly attenuated apoptotic signals in the diabetic heart in mice fed with HFD (0.16 % in HFD +butyrate group, $p<0.001$vs. HFD.) (Figures 5A and 5B). Likewise, active caspase-3 was elevated in HDF-treated mice, which was suppressed by sodium butyrate (Figure 5C). As shown in Figures 5D and 5E, HFD-induced diabetic hearts showed significantly enhanced superoxide production detected by DHE staining as compared to hearts of chow-fed mice, but this effect was partially prevented by the administration of sodium butyrate, suggesting that the inhibition of HDAC reduces HFD-induced oxidative stress in mice hearts. The lipid accumulation demonstrated increases in muscle and heart under obesity-induced metabolic stress as compared to chow control (Figure 6A and B). HDAC inhibition significantly suppressed lipid accumulation in HFD-fed animals. Furthermore, we determine whether HDAC inhibition reverses HFD induced white fat cell hypertrophy.

Sodium butyrate treatment induces cardiac angiogenesis

Immunofluorescent staining of CD31 was performed to examine the angiogenetic responses to HFD and inhibition of HDAC. As shown in Figures 7A and 7B, CD31 positive capillary density in the myocardium was decreased in myocardium of HFD-fed mice as compared with both chow groups ($155.36\pm23.46/mm^2$ in HFD group, $263.42\pm18.54/mm^2$ in chow group, $256.79\pm29.83/mm^2$ in chow+butyrate group). Administration of sodium butyrate substantially increased the capillary density in myocardium of HFD-fed mice ($260.56\pm23.00/mm^2$, $p<0.05$ vs. HFD).

Effects of Sodium butyrate treatment on kinase phosphorylation

As shown in Figures 8A and B relative to other HDAC isoforms, HDAC4 protein was dramatically elevated in the myocardium of HFD group, which was significantly attenuated following HDAC inhibition. Other HDAC isoforms (HDACs 1, 2, 3 and 10) were not affected by HDAC inhibition. Interestingly, HDAC4 displays abundant accumulations in the section of myocardium in HFD-treated mice (Figure 8C). The stained HDAC4 positive signals in HFD treated mice were reduced by sodium butyrate, indicating that HDAC4 may be more sensitive to HFD-induced diabetic heart failure and HDAC inhibition. HDAC activity was elevated in the myocardium of HFD-fed mice, which was significantly reduced by sodium butyrate (Figure 8D). Notably, butyrate treatment increased the levels of both MKK3 and p38 phosphorylation, whereas HFD demonstrated a decrease in phosphorylation of MKK3 and p38, which were prevented by sodium butyrate (Figure 8E and F). Phosphorylation of PRAK, a downstream target of p38, was also decreased in HFD-fed mice, but sodium butyrate prevented the reduction of phosphorylated PRAK (Figure 8G). Additionally, HFD also induced the suppression of Ak-1 phosphorylation, which was prevented by sodium butyrate (Figure 8H). However, phosphorylated p44/42 was not affected significantly in HFD as well as by sodium butyrate treatment (Figure 8I), suggesting that the protective effects of sodium butyrate are related to activation of the MKK3/p38/PRAK signaling pathway.

DISCUSSION

In this study, we evaluated the effects of HDAC inhibition on the HFD-induced myocardial dysfunction in obesity-induced metabolic stress. We demonstrated that HDAC inhibition reversed hyper-cholesterolemia, glucose intolerance, and metabolic disturbance caused by high fat diets. Furthermore, we showed that HDAC inhibition played a pivotal role in mitigating impaired cardiac function, cardiac remodeling, increased apoptosis, enhanced oxidative stress, and lipid accumulations in the HFD-fed mice. In addition, HDAC inhibition prevented the deficiency in cardiac angiogenesis induced by obesity and diabetes. Notably, as the new MKK3/p38/PRAK signaling pathway was attenuated in HFD, sodium butyrate treatment significantly activates the phosphorylation of MKK3/P38/PRAK. To the best of our acknowledge, these findings are the first demonstration to reveal that HDAC inhibition preserves myocardial performance, suppresses cardiac remodeling, and attenuates metabolic disorders in diabetic and obese mice.

We and other investigators revealed that HDAC inhibitors elicited cardioprotective effects against cellular and myocardial ischemic injuries and hypertrophy (Du J et al., 2015; Gallo P et al., 2008; Kee HJ et al., 2006;, Kong Y et al., 2006; Nural-Guvener H et al., 2015;, Wang J et al., 2015). Very recently, the approach to targeting HDAC has attracted dramatic attention to exploring a potential therapy for diabetic complications and obesity (Newman JC & Verdin E. 2014). Studies from other groups indicate that HDAC inhibition is critical to suppressing the magnitude of metabolic disturbance (Gao Z et al., 2009; Khan S & Jena G, 2016). However, the effect of HDAC inhibition on the attenuation of cardiac dysfunction remains unclear in HFD-induced type II diabetes and obesity. More importantly, we have recently indicated that HDAC inhibition demonstrated protective effects in type I diabetic model (Chen Y et al., 2015). However, whether or not HDAC inhibition could prevent cardiac dysfunction in high fat diet-induced-type II diabetes and obesity and alter the signaling pathway following HDAC inhibition needs to be determined.

Clinical studies demonstrate that diabetes mellitus increased the susceptibility of the myocardium to ischemic injury (Busche MN et al., 2008; Regan TJ et al., 1977). We have demonstrated that the diabetic heart presents progressive LV systolic failure following feeding of mice with a HFD for 24 weeks, which is consistent with observations in the development of cardiac dysfunction in HFD-induced diabetic mice (Völkers M et al., 2014). Sodium butyrate, a potent HDAC inhibitor, effectively demonstrated cardioprotection in our previous studies (Du J et al., 2015), and that butyrate could serve as a promising approach to treating diabetic complications (Newman JC & Verdin E., 2014). HDAC inhibition prevented diet-induced obesity and insulin resistance (Gao Z et al., 2009). We found that HDAC inhibition effectively prevented body weight gain, attenuated hyperinsulinemia, hyperglycemia, triglycerides, and attenuated whole body insulin resistance in the HFD mice, implying that HDAC inhibition exerts a robust protective effect against HFD-induced metabolic dysfunction. The effect of attenuating glucose tolerance by HDAC inhibition is also supported by a recent observation in which glucose homeostasis was improved by sodium butyrate in juvenile diabetic rat (Khan S & Jena G, 2016). It was reported that food intake was increased with sodium butyrate in different strain of mice. Furthermore, sodium butyrate did not affect food consumption of HFD-induced obesity (Henagan TM et al, 2015)

mice. We have noticed that the short-term taking of sodium butyrate did not affect either water or food intake (data not shown), suggesting that food intake may not be a reason for the attenuation of body weight in this event. However, water intake and food intake during the studies were not evaluated in this observation, which is a limitation for the study. An important pathological feature of diabetic cardiomyopathy is cardiac hypertrophy (Lieb W et al., 2009). More importantly, HDAC inhibition was reported to block myocardial hypertrophy, induced by angiotensin II infusion and aortic banding (Haberland M et al., 2009; Kee HJ et al., 2006). Our observation revealed that HDAC inhibition prevented these hypertrophic features in the myocardium of HFD-fed mice, which is supported by our recent observation in which cardiac hypertrophy and fibrosis were mitigated in the infarcted hearts following global HDAC inhibition (Zhang L et al., 2012). Another observed feature of HFD-fed mice is the remarkable increase in apoptotic positive myocytes in the hearts, which was also suppressed by administering sodium butyrate. Oxidative stress has been suggested by several studies to be an underlying factor in hyperglycemia-induced myocardial cell deaths (Nakamura H et al., 2012). We found that HFD-induced diabetes resulted in a significant increase in superoxide production in the myocardium, which was also mitigated by inhibition of HDAC, suggesting an important link between HDAC inhibition and prevention of superoxide production. The reductions in capillary and arteriolar densities were shown in the myocardial infarction model of diabetic conditions. The present observation indicates the reduction of vascular density from HFD-fed mice, which was prevented by HDAC inhibition in diabetic mice. This is consistent with our recent findings that HDAC inhibition stimulated endogenous angiomyogenesis in myocardial infarcted models (Zhang L et al., 2012).

We have previously shown that HDAC inhibition-induced protective effects is closely related to the reduction of HDAC4 in infarcted hearts (Chen HP et al., 2011). HFD-induced diabetic mice displayed an increase in HDAC4 protein, but not in other HDAC isoforms. Sodium butyrate exclusively prevented the increase in HDAC4 in myocardium of HFD-fed mice, suggesting that HDAC4 may involve the protective effect of sodium butyrate in diabetic and obese mice. It will be interesting to see the effects of HDAC4 in modulating cardiac function and metabolic disturbances under these conditions when a specific HDAC4 inhibitor is available. In addition, the specific inhibition of other HDACs was reported to reduce hyperglycemia and increase insulin secretion in a rat model of type 2 diabetes (Lundh M et al, 2015; Meier BC& Wagner BK. 2014). It will be important to determine how different HDAC isoforms modulate the development of metabolic disorders and cardiac myopathy in these models. Previous work has demonstrated that p38 phosphorylation was closely associated with insulin improvement and beneficial effects in diabetic hearts (1 Bhashyam S et al., 2010; Zhao T et al., 2006). We have also demonstrated that genetic inhibition of MKK3/p38 and Akt-1 abolished the protective effects of GLP-1 receptor-induced protective effects (Du J et al., 2016). In this observation, we found that a high fat diet induced the attenuation of phosphorylated MKK3 and p38, which were prevented by supplying sodium butyrate. Additionally, the high fat diet suppressed the phosphorylation levels of PRAK, which is an identified p38 substrate and was found to attenuate insulin resistance (Zheng M et al., 2011). Sodium butyrate augmented PRAK phosphorylation, indicating that HDAC inhibition induced an activation of MKK3/p38/PRAK and Akt-1 pathway in mediating metabolic control and cardiac function. Since both p38 and PRAK were subjected to

acetylation, it is also likely that HDAC inhibition following sodium butyrate stimulates acetylation of MKK3/p38/PRAK. Furthermore, it will be interesting to investigate whether there exists a cascade of p38 and Akt1 in the HFD-fed condition. Additionally, there are no significant changes in ERK in these conditions, indicating that Erk signaling pathways may not be major signaling involved. In addition, a milk fat diet is considered to be a Western diet, which has been utilized in the study of diabetes and obesity (Wagner EM et al., 2008). It is not clear whether HDAC inhibition will respond differently to milk fat diet-induced diabetes models, which merits future investigation.

In summary, this is the first evidence to demonstrate that HDAC inhibition protects against HFD-induced cardiac dysfunction and metabolic dysfunction HFD-induced type II diabetes. HDAC inhibition reversed ventricular dysfunction, attenuated cardiac remodeling and interstitial fibrosis, which are associated with reduction of myocyte apoptosis. Hyperinsulinemia, hyperglycemia, and lipid accumulations induced by a high fat diet was also diminished by inhibition of HDACs. Notably, the HFD-induced diabetic myocardium displayed a decrease in vascular density, which was prevented by inhibition of HDAC. We showed that the protective effects of HDAC inhibition resulted in activations of PRAK signaling pathways. To the best of our knowledge, this is the first demonstration of the protective effects of HDAC inhibition against HFD-induced cardiac dysfunction and metabolic disturbance in the type II diabetic and obese model involving PRAK pathway. Our study holds promise in developing a therapeutic approach to target HDAC and treat diabetic patients.

Acknowledgments

Funding resources: The work is supported by the National Heart, Lung, and Blood Institute Grant (R01 HL089405 and R01 HL115265)

References

1. Bhashyam S, Fields AV, Patterson B, Testani JM, Chen L, Shen YT, Shannon RP. Glucagon-like peptide-1 increases myocardial glucose uptake via p38alpha MAP kinase-mediated, nitric oxide-dependent mechanisms in conscious dogs with dilated cardiomyopathy. Circ Heart Fail. 2010; 4:512–21.
2. Busche MN, Walsh MC, McMullen ME, Guikema BJ, Stahl GL. Mannose-binding lectin plays a critical role in myocardial ischaemia and reperfusion injury in a mouse model of diabetes. Diabetologia. 2008; 51:1544–51. [PubMed: 18493734]
3. Chen Y, Du J, Zhao YT, Zhang L, Lv G, Zhuang S, Qin G, Zhao TC. Histone deacetylase (HDAC) inhibition improves myocardial function and prevents cardiac remodeling in diabetic mice. Cardiovasc Diabetol. 2015; 14:99. [PubMed: 26245924]
4. Chen HP, Denicola M, Qin X, Zhao Y, Zhang L, Long XL, Zhuang S, Liu PY, Zhao TC. HDAC inhibition promotes cardiogenesis and the survival of embryonic stem cells through proteasome-dependent pathway. J Cell Biochem. 2011; 112:3246–55. [PubMed: 21751234]
5. Cook S, Hugli O, Egli M, Ménard B, Thalmann S, Sartori C, Perrin C, Nicod P, Thorens B, Vollenweider P, Scherrer U, Burcelin R. Partial gene deletion of endothelial nitric oxide synthase predisposes to exaggerated high-fat diet-induced insulin resistance and arterial hypertension. Diabetes. 2004; 53:2067–72. [PubMed: 15277387]
6. Du J, Zhang L, Zhuang S, Qin GJ, Zhao TC. HDAC4 degradation mediates HDAC inhibition-induced protective effects against hypoxia/reoxygenation injury. J Cell Physiol. 2015; 230:1321–31. [PubMed: 25475100]

7. Du J, Zhang L, Wang Z, Yano N, Zhao YT, Wei L, Dubielecka-Szczerba P, Liu PY, Zhuang S, Qin G, Zhao TC. Exendin-4 induces myocardial protection through MKK3 and Akt-1 in infarcted hearts. Am J Physiol Cell Physiol. 2016; 310:C270–83. [PubMed: 26739490]
8. Gallo P, Latronico MV, Gallo P, Grimaldi S, Borgia F, Todaro M, Jones P, Gallinari P, De Francesco R, Ciliberto G, Steinkühler C, Esposito G, Condorelli G. Inhibition of class I histone deacetylase with an apicidin derivative prevents cardiac hypertrophy and failure. Cardiovasc Res. 2008; 80:416–424. [PubMed: 18697792]
9. Galmozzi A, Mitro N, Ferrari A, Gers E, Gilardi F, Godio C, Cermenati G, Gualerzi A, Donetti E, Rotili D, Valente S, Guerrini U, Caruso D, Mai A, Saez E, De Fabiani E, Crestani M. Inhibition of class I histone deacetylases unveils a mitochondrial signature and enhances oxidative metabolism in skeletal muscle and adipose tissue. Diabetes. 2013; 62:732–42. [PubMed: 23069623]
10. Gao Z, Yin J, Zhang J, Ward RE, Martin RJ, Lefevre M, Cefalu WT, Ye J. Butyrate improves insulin sensitivity and increases energy expenditure in mice. Diabetes. 2009; 58:1509–17. [PubMed: 19366864]
11. Haberland M, Montgomery RL, Olson EN. The many roles of histone deacetylases in development and physiology: implications for disease and therapy. Nat Rev Genet. 2009; 10:32–42. [PubMed: 19065135]
12. Henagan TM, Stefanska B, Fang Z, Navard AM, Ye J, Lenard NR, Devarshi PP. Sodium butyrate epigenetically modulates high-fat diet-induced skeletal muscle mitochondrial adaptation, obesity and insulin resistance through nucleosome positioning. Br J Pharmacol. 2015; 172:2782–98. [PubMed: 25559882]
13. Kang JS, Lee WK, Lee CW, Yoon WK, Kim N, Park SK, Lee HS, Park HK, Han SB, Yun J, Lee K, Lee KH, Park SK, Kim HM. Improvement of high-fat diet-induced obesity by a mixture of red grape extract, soy isoflavone and L-carnitine: implications in cardiovascular and non-alcoholic fatty liver diseases. Food Chem Toxicol. 2011; 49:2453–58. [PubMed: 21745528]
14. Kee HJ, Sohn IS, Nam KI, Park JE, Qian YR, Yin Z, Ahn Y, Jeong MH, Bang YJ, Kim N, Kim JK, Kim KK, Epstein JA, Kook H. Inhibition of histone deacetylation blocks cardiac hypertrophy induced by angiotensin II infusion and aortic banding. Circulation. 2006; 113:51–9. [PubMed: 16380549]
15. Khan S, Jena G. Sodium butyrate reduces insulin-resistance, fat accumulation and dyslipidemia in type-2 diabetic rat: A comparative study with metformin. Chem Biol Interact. 2016; 254:124–34. [PubMed: 27270450]
16. Khan S, Jena G. The role of butyrate, a histone deacetylase inhibitor in diabetes mellitus: experimental evidence for therapeutic intervention. Epigenomics. 2015; 7:669–80. [PubMed: 26111036]
17. Kong Y, Tannous P, Lu G, Berenji K, Rothermel BA, Olson EN, Hill JA. Suppression of class I and II histone deacetylases blunts pressure-overload cardiac hypertrophy. Circulation. 2006; 113:2579–88. [PubMed: 16735673]
18. Kurdi M, Booz GW. Three 4-letter words of hypertension-related cardiac hypertrophy: TRPC, mTOR, and HDAC. J Mol Cell Cardiol. 2011; 50:964–71. [PubMed: 21320507]
19. Lamounier-Zepter V, Look C, Alvarez J, Christ T, Ravens U, Schunck WH, Ehrhart-Bornstein M, Bornstein SR, Morano I. Adipocyte fatty acid-binding protein suppresses cardiomyocyte contraction: a new link between obesity and heart disease. Circ Res. 2009; 105:326–34. [PubMed: 19608978]
20. Lieb W, Xanthakis V, Sullivan LM, Aragam J, Pencina MJ, Larson MG, Benjamin EJ, Vasan RS. Longitudinal tracking of left ventricular mass over the adult life course: clinical correlates of short- and long-term change in the Framingham offspring study. Circulation. 2009; 119:3085–92. [PubMed: 19506113]
21. Lundh M, Galbo T, Poulsen SS, Mandrup-Poulsen T. Histone deacetylase 3 inhibition improves glycaemia and insulin secretion in obese diabetic rats. Diabetes Obes Metab. 2015; 17(7):703–7. [PubMed: 25846481]
22. Meier BC, Wagner BK. Inhibition of HDAC3 as a strategy for developing novel diabetes therapeutics. Epigenomics. 2014; 6(2):209–14. [PubMed: 24811789]

23. Nakamura H, Matoba S, Iwai-Kanai E, Kimata M, Hoshino A, Nakaoka M, Katamura M, Okawa Y, Ariyoshi M, Mita Y, Ikeda K, Okigaki M, Adachi S, Tanaka H, Takamatsu T, Matsubara H. p53 promotes cardiac dysfunction in diabetic mellitus caused by excessive mitochondrial respiration-mediated reactive oxygen species generation and lipid accumulation. Circ Heart Fail. 2012; 5:106–15. [PubMed: 22075967]
24. Newman JC, Verdin E. β-hydroxybutyrate: much more than a metabolite. Diabetes Res Clin Pract. 2014; 106:173–81. [PubMed: 25193333]
25. Nural-Guvener H, Zakharova L, Feehery L, Sljukic S, Gaballa M. Anti-Fibrotic Effects of Class I HDAC Inhibitor, Mocetinostat Is Associated with IL-6/Stat3 Signaling in Ischemic Heart Failure. Int J Mol Sci. 2015; 16:11482–99. [PubMed: 25997003]
26. Odermatt A. The Western-style diet: a major risk factor for impaired kidney function and chronic kidney disease. Am J Physiol Renal Physiol. 2011; 301(5):F919–31. [PubMed: 21880837]
27. Olson EN, Backs J, McKinsey TA. Control of cardiac hypertrophy and heart failure by histone acetylation/deacetylation. Novartis Found Symp. 2006; 274:3–12. [PubMed: 17019803]
28. Olsson B, Bohlooly-Y M, Fitzgerald SM, Frick F, Ljungberg A, Ahrén B, Törnell J, Bergström G, Oscarsson J. Bovine growth hormone transgenic mice are resistant to diet-induced obesity but develop hyperphagia, dyslipidemia, and diabetes on a high-fat diet. Endocrinology. 2015; 146:920–30.
29. Relling DP, Esberg LB, Fang CX, Johnson WT, Murphy EJ, Carlson EC, Saari JT, Ren J. High-fat diet-induced juvenile obesity leads to cardiomyocyte dysfunction and upregulation of Foxo3a transcription factor independent of lipotoxicity and apoptosis. J Hypertens. 2006; 24:549–61. [PubMed: 16467659]
30. Regan TJ, Lyons MM, Ahmed SS, Levinson GE, Oldewurtel HA, Ahmad MR, Haider B. Evidence for cardiomyopathy in familial diabetes mellitus. J Clin Invest. 1977; 60:884–99. [PubMed: 893679]
31. Shulman GI. Ectopic fat in insulin resistance, dyslipidemia, and cardiometabolic disease. N Engl J Med. 2014; 371:1131–41. [PubMed: 25229917]
32. Sun H, Yang X, Zhu J, Lv T, Chen Y, Chen G, Zhong L, Li Y, Huang X, Huang G, Tian J. Inhibition of p300-HAT results in a reduced histone acetylation and down-regulation of gene expression in cardiac myocytes. Life Sci. 2010; 87:707–714. [PubMed: 21034749]
33. Update on Prevention of Cardiovascular Disease in Adults With Type 2 Diabetes Mellitus in Light of Recent Evidence: A Scientific Statement From the American Heart Association and the American Diabetes Association. Circulation. 2015; 132(8):691–718. [PubMed: 26246173]
34. Völkers M, Doroudgar S, Nguyen N, Konstandin MH, Quijada P, Din S, Ornelas L, Thuerauf DJ, Gude N, Friedrich K, Herzig S, Glembotski CC, Sussman MA. PRAS40 prevents development of diabetic cardiomyopathy and improves hepatic insulin sensitivity in obesity. EMBO Mol Med. 2014; 6:57–65. [PubMed: 24408966]
35. Wagner EM, Jen KL, Artiss JD, Remaley AT. Dietary alpha-cyclodextrin lowers low-density lipoprotein cholesterol and alters plasma fatty acid profile in low-density lipoprotein receptor knockout mice on a high-fat diet. Metabolism. 2008; 57(8):1046–51. [PubMed: 18640380]
36. Wang J, Hu X, Jiang H. HDAC inhibition: A novel therapeutic target for attenuating myocardial ischemia and reperfusion injury by reversing cardiac remodeling. Int J Cardiol. 2015; 190:126–127. [PubMed: 25918063]
37. Ye J. Improving insulin sensitivity with HDAC inhibitor. Diabetes. 2013; 62:685–7. [PubMed: 23431009]
38. Zhang L, Chen B, Zhao Y, Dubielecka PM, Wei L, Qin GJ, Chin YE, Wang Y, Zhao TC. Inhibition of histone deacetylase-induced myocardial repair is mediated by c-kit in infarcted hearts. J Biol Chem. 2012; 287:39338–48. [PubMed: 23024362]
39. Zhang L, Qin X, Zhao Y, Fast L, Zhuang S, Liu P, Cheng G, Zhao TC. Inhibition of histone deacetylases preserves myocardial performance and prevents cardiac remodeling through stimulation of endogenous angiomyogenesis. J Pharmacol Exp Ther. 2012; 341:285–93. [PubMed: 22271820]

40. Zhao T, Parikh P, Bhashyam S, Bolukoglu H, Poornima I, Shen YT, Shannon RP. Direct effects of glucagon-like peptide-1 on myocardial contractility and glucose uptake in normal and postischemic isolated rat hearts. J Pharmacol Exp Ther. 2006; 317:1106–13. [PubMed: 16489128]

41. Zheng M, Wang YH, Wu XN, Wu SQ, Lu BJ, Dong MQ, Zhang H, Sun P, Lin SC, Guan KL, Han J. Inactivation of Rheb by PRAK-mediated phosphorylation is essential for energy-depletion-induced suppression of mTORC1. Nat Cell Biol. 2011; 13:263–72. [PubMed: 21336308]

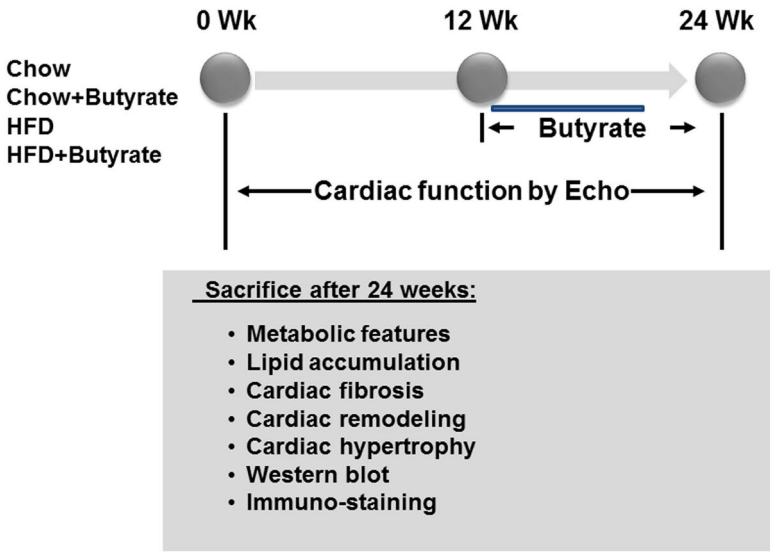

Figure 1.

Schemas of animal experimentation in high-fat diet (HFD) versus Chow control diet. Echo: echocardiography; Detailed descriptions of the experiments are listed in the section of Methods (n=5 per group).

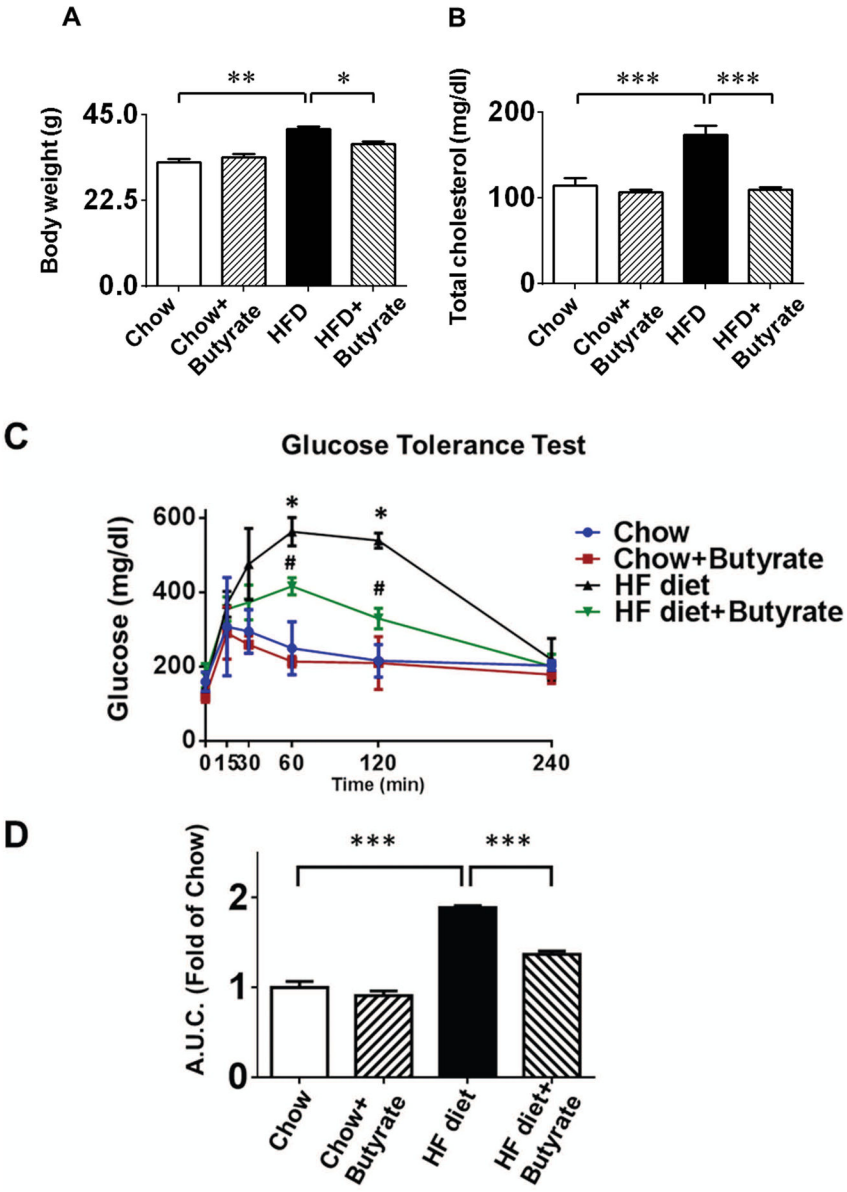

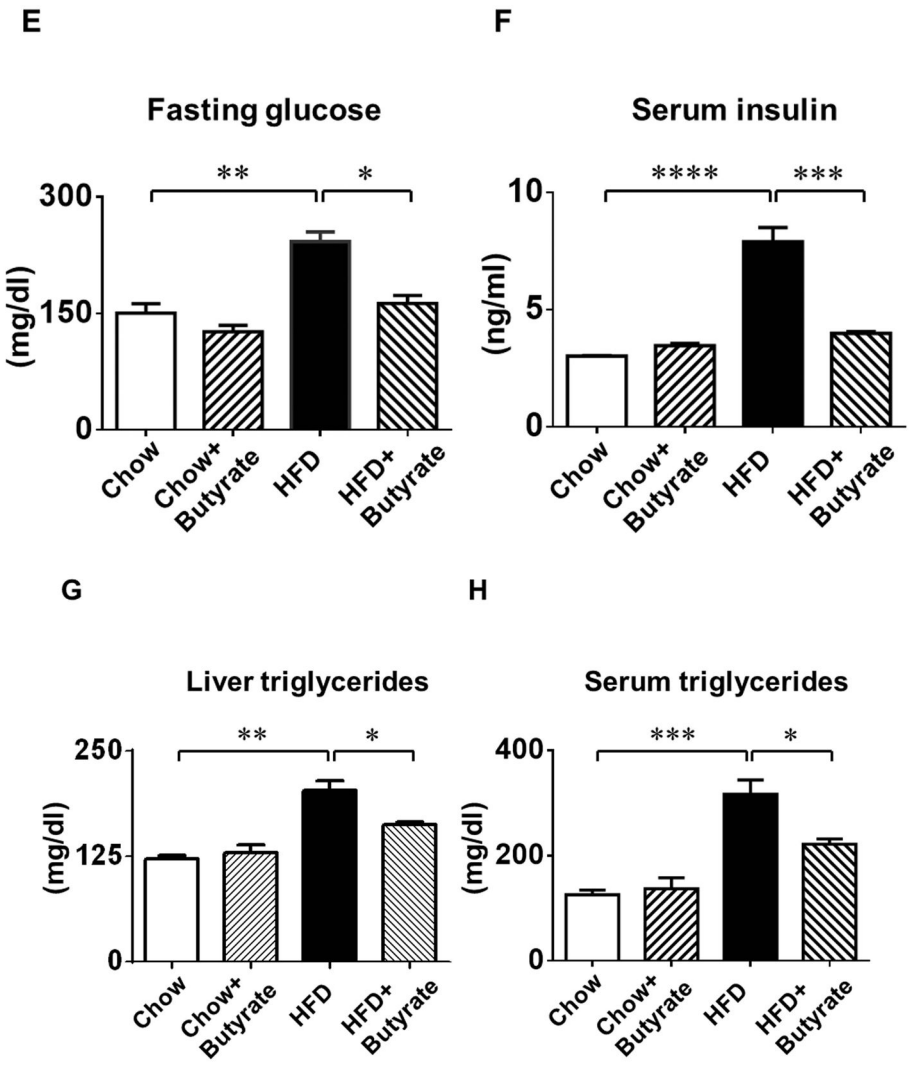

Figure 2. Sodium butyrate treatment attenuates diet-induced metabolic syndrome in obese mice

A: Body weights and **B:** total blood cholesterol of mice fed with standard chow or HFD after 24 weeks. Data are shown as means ± SEM. ***** $p<0.05$, ****** $p<0.01$, ******* $p<0.001$. **C.** Glucose tolerance test. ***** $p<0.05$ vs. Chow; # $p<0.05$ vs. HFD. **D:** Area under curve for GTT. * $p<0.05$. (n=4–5 per group). **E**: Fasting glucose; **F**: Serum insulin; **G**: Liver triglycerides; **H**: Blood triglycerides; ***** $p<0.05$, ****** $p<0.01$, ******* $p<0.001$ (n=3–5 per group from E to H).

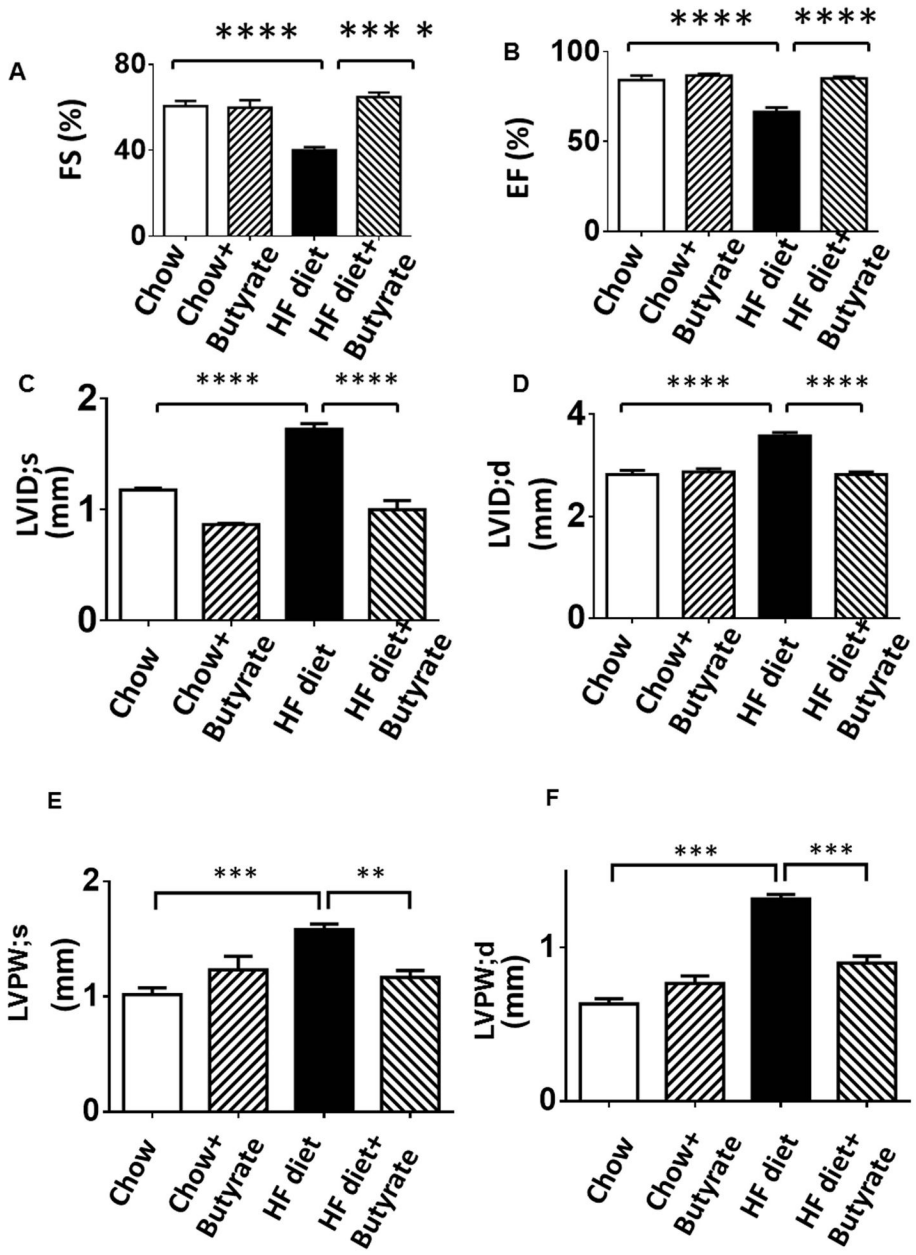

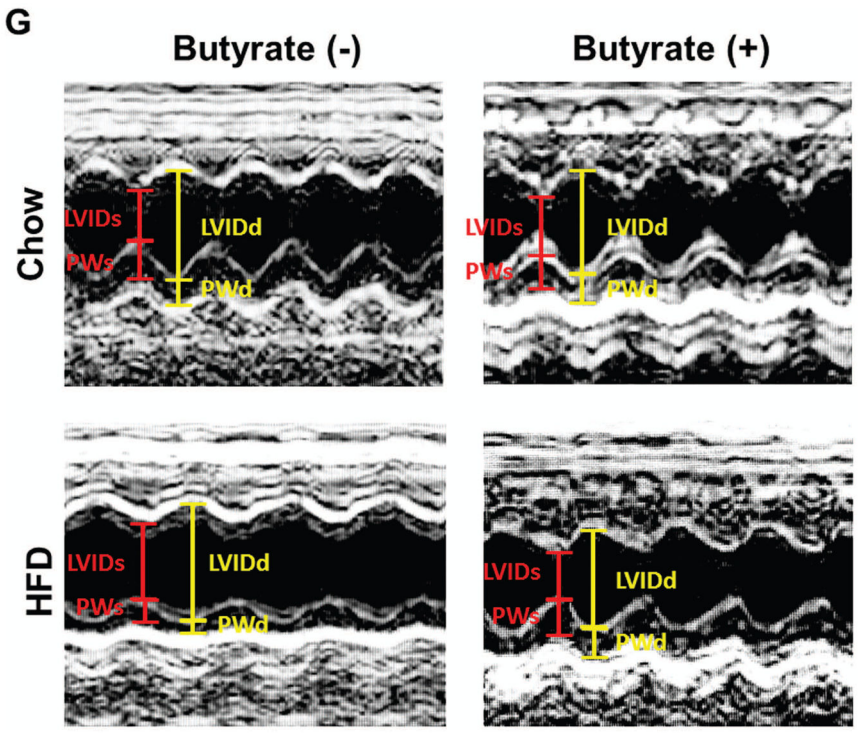

Figure 3. Sodium butyrate treatment improved impaired left ventricular function in HFD-fed mice

Echocardiographic measurements of ventricular functional parameters includes **A**: Fractional Shortening (FS) **B**: Ejection Fraction (EF); **C**. Left Ventricular Internal Dimension in Diastole (LVID;d); **D**: Left Ventricular Internal Dimension in Systole (LVID;s); **E and F**: Left ventricular posterior wall (LVPW;s and LVPW;d); **G**: Representative image of M-mode. Data are shown as means ± SEM (n=4–5 per group). ** p<0.01, *** p<0.001, **** p<0.0001.

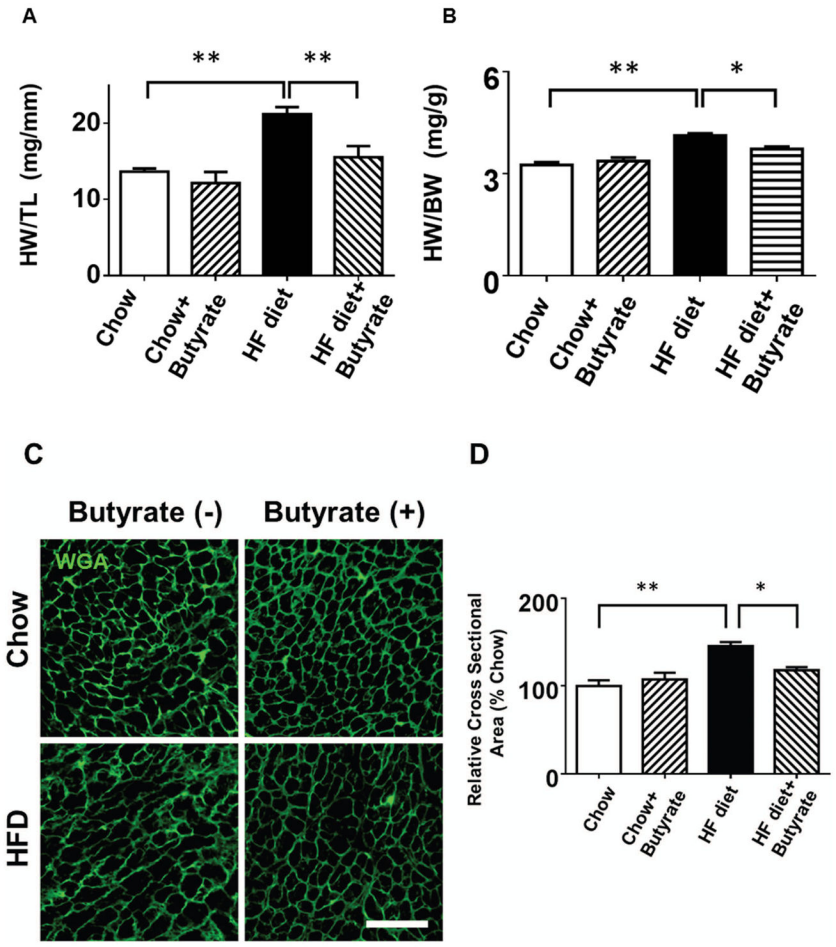

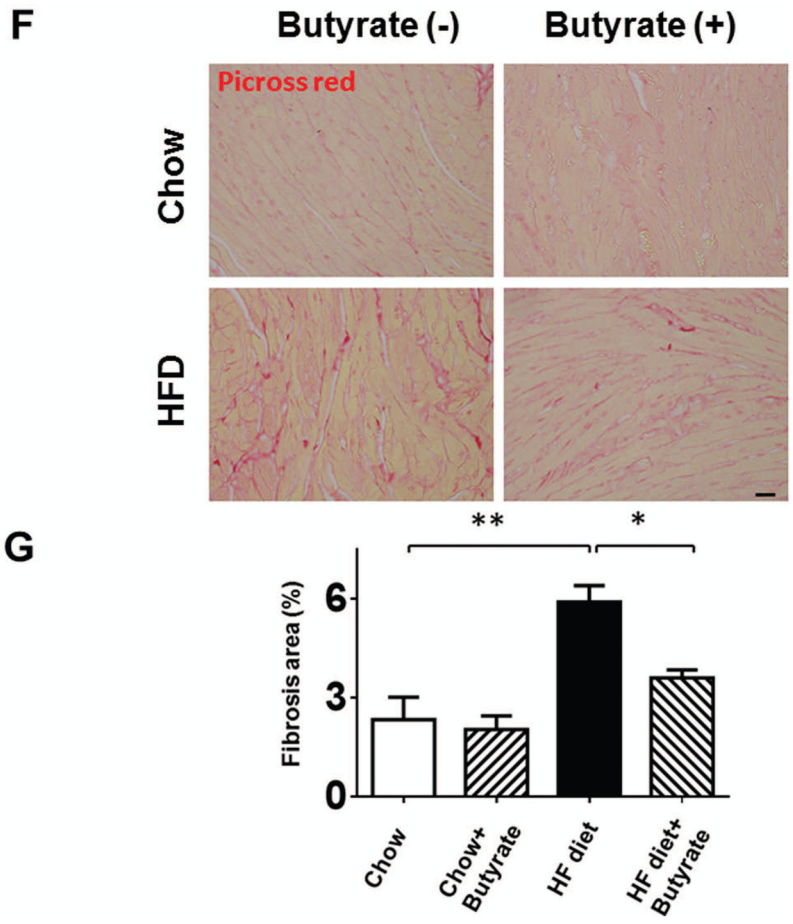

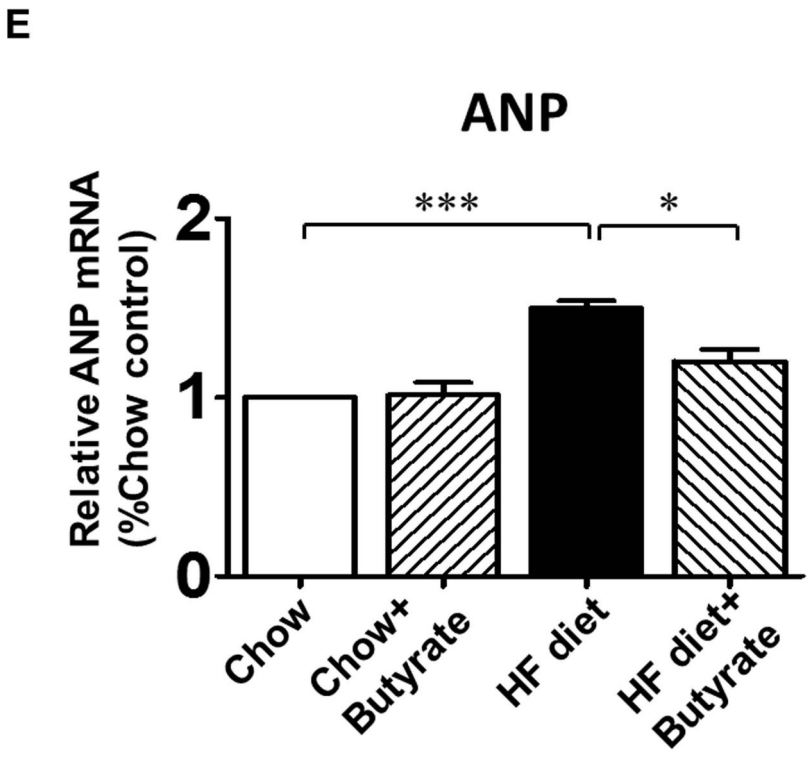

Figure 4. Effect of sodium butyrate on HFD-induced structural remodeling

A. The ratio of heart weight to tibia length; **B**: Heart weight/body weight ratio; **C.** Representative images of wheat germ agglutinin (WGA) staining (scale bar: 100μm). **D:** Quantitative analysis of myocyte cross-sectional area (n=4–5 per group). **E**: mRNA levels of ANP genes in heart (n=3 heart per group). **F:** Representative images of picrosirius red staining (scale bar: 50 um). **G.** Quantitative analysis of myocardial interstitial collagen deposition (n=4 per group). Data are shown as means ± SEM. ***p*<0.05, ****p*<0.01.

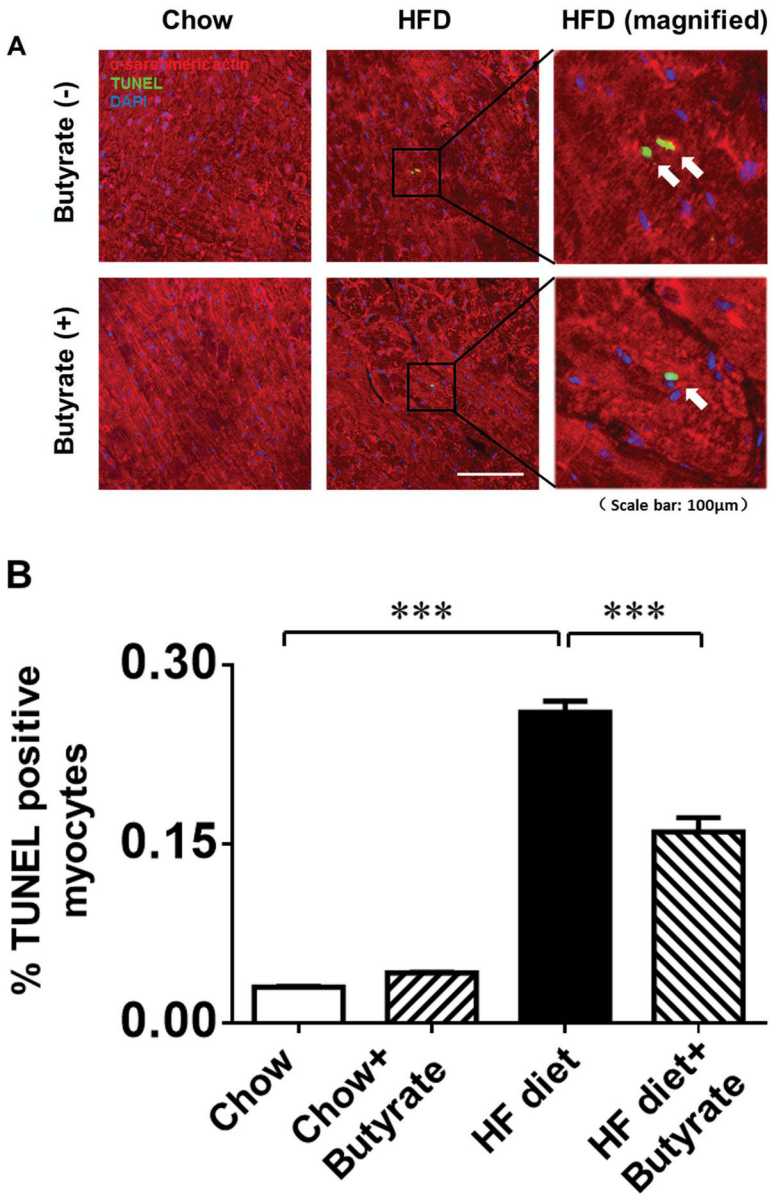

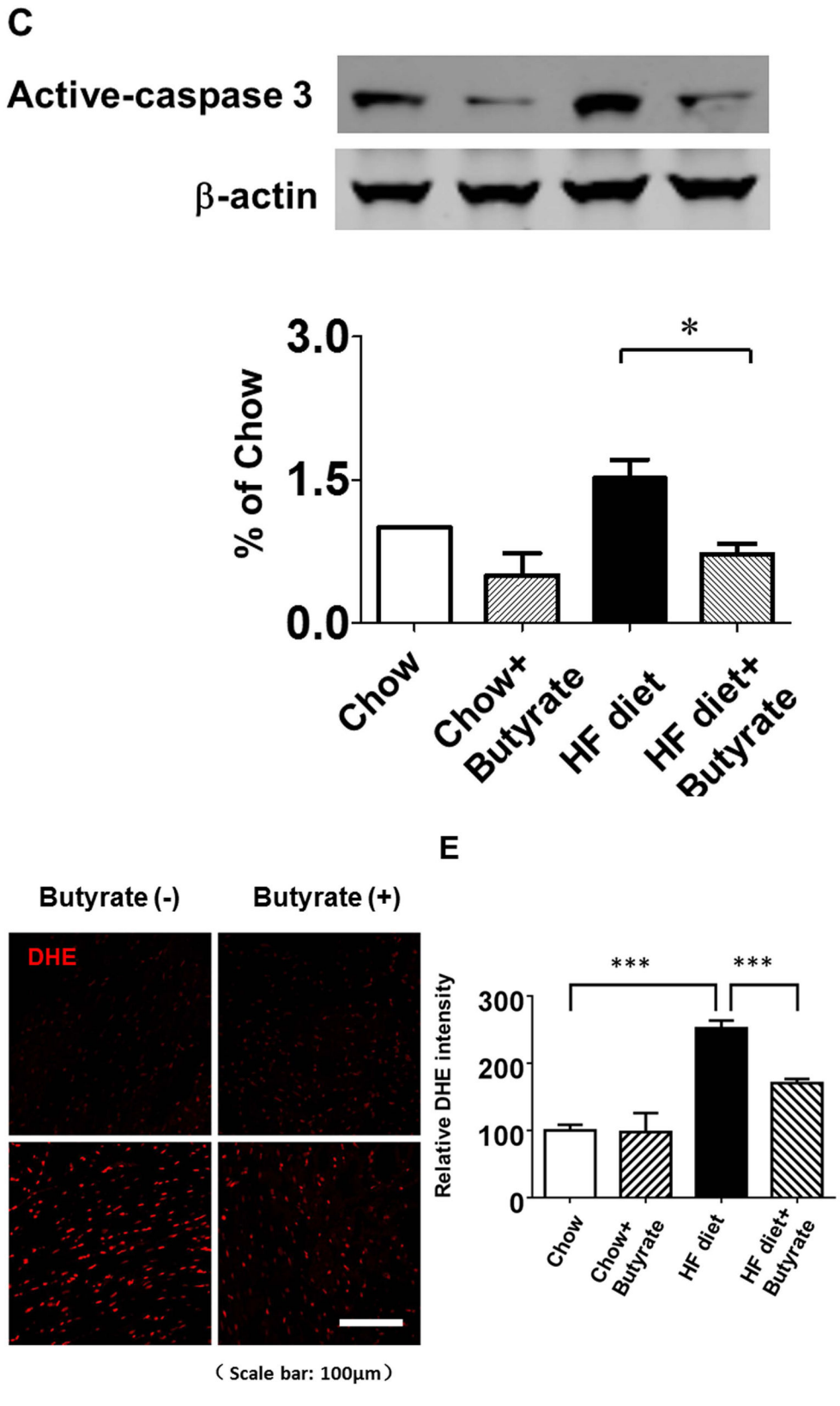

Figure 5. Sodium butyrate treatment reduced apoptosis and oxidative stress in HFD-induced diabetic heart

A: Representative images of TUNEL (Green: TUNEL positive staining; Red: α-sarcomeric actin; Blue: DAPI). **B:** Quantitative analysis of TUNEL-positive nuclei. Values are shown as mean ± SEM (n = 4–5 per group); *** $p<0.001$. **C**: Western blot showing sodium butyrate attenuated active-caspase 3 in HFD-fed mice. The bar graph shows the densitometric scanning results (means ± SEM) (n=3 per group), ***$p<0.05$. **D:** Representative images of DHE staining. **E:** Quantitative analysis of fluorescence intensity of DHE staining (n = 3–5 per group); **** $p<0.001$. Scale bar: 100μm. DHE: Dihydroethidium.

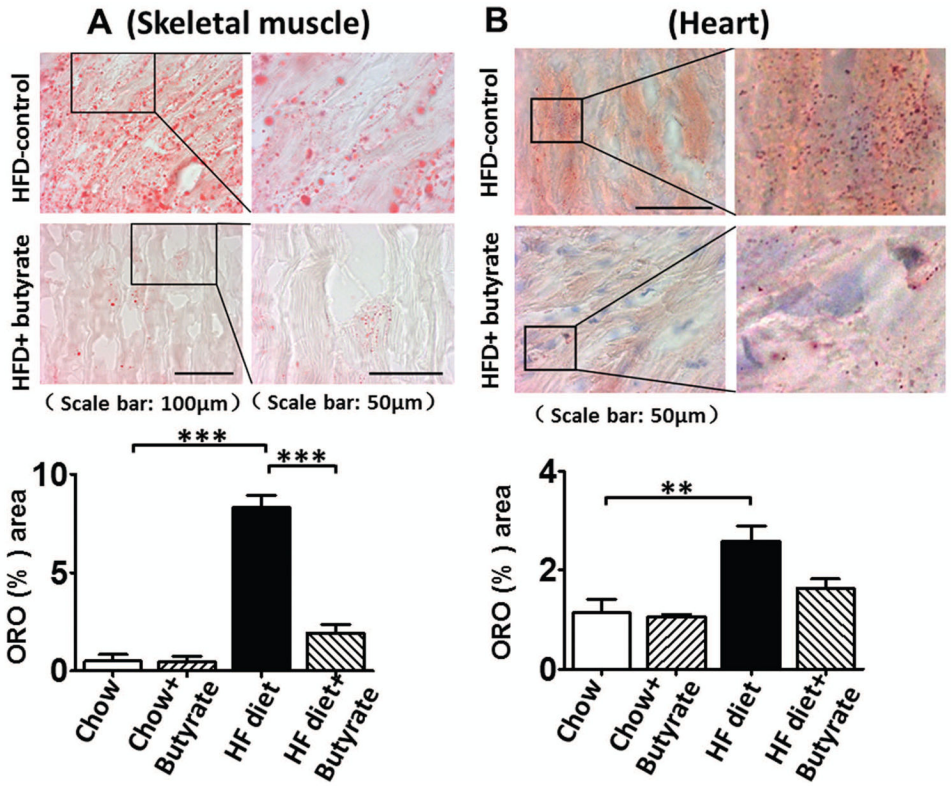

Figure 6. Sodium butyrate treatment attenuated lipid accumulations and suppressed hypertrophy of adipocytes

A: Representative images of Oil Red O staining and quantitative analysis of lipid contents in skeletal muscle; **B**: Representative images of Oil Red O staining and quantitative analysis of lipid contents in myocardium (n=3–4/per group). Values are shown as mean ± SEM, ***** $p < 0.05$**, **** $p<0.01$, *****$p<0.001$.

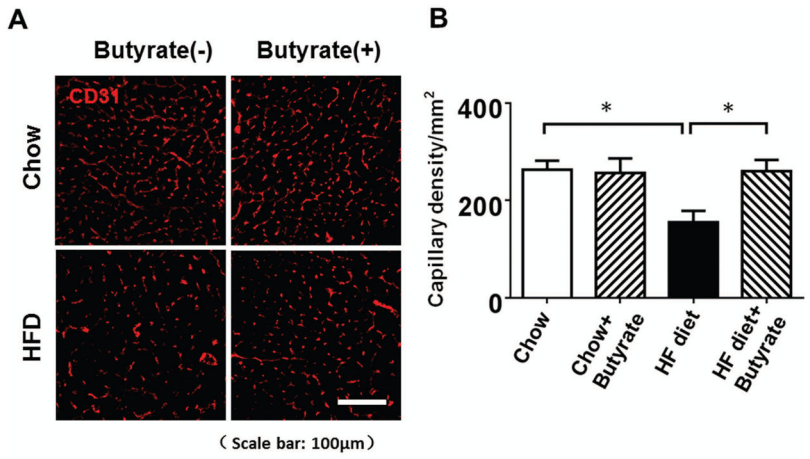

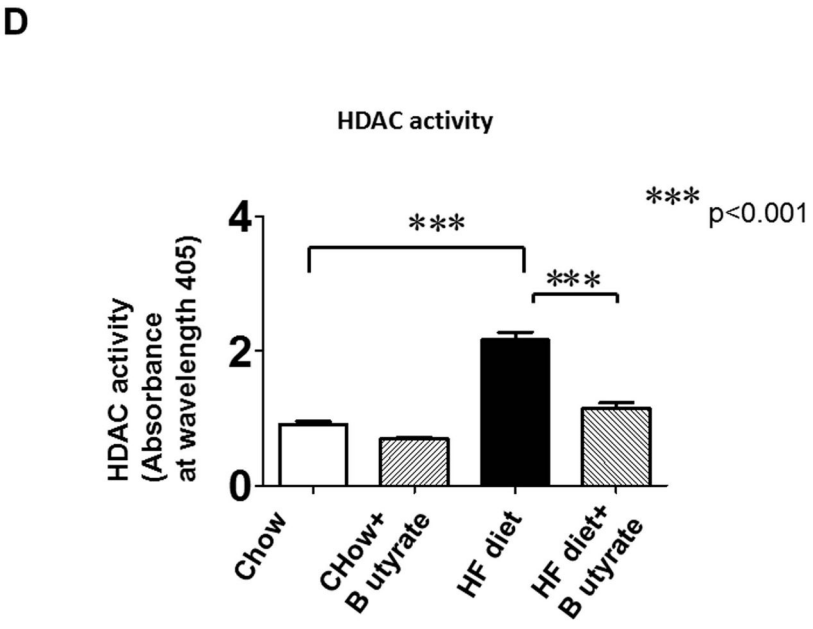

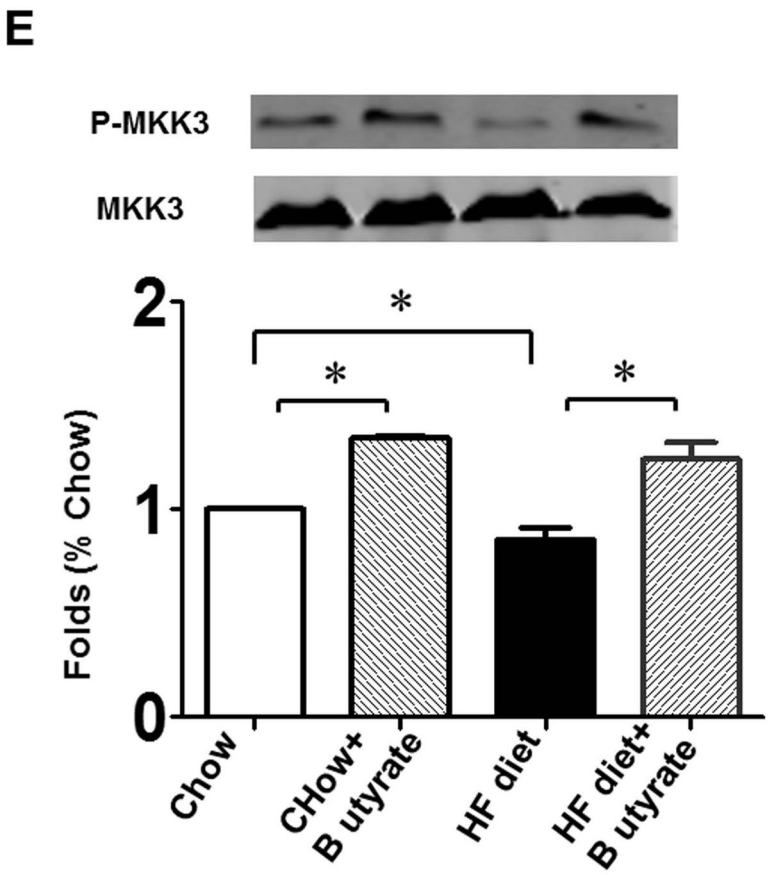

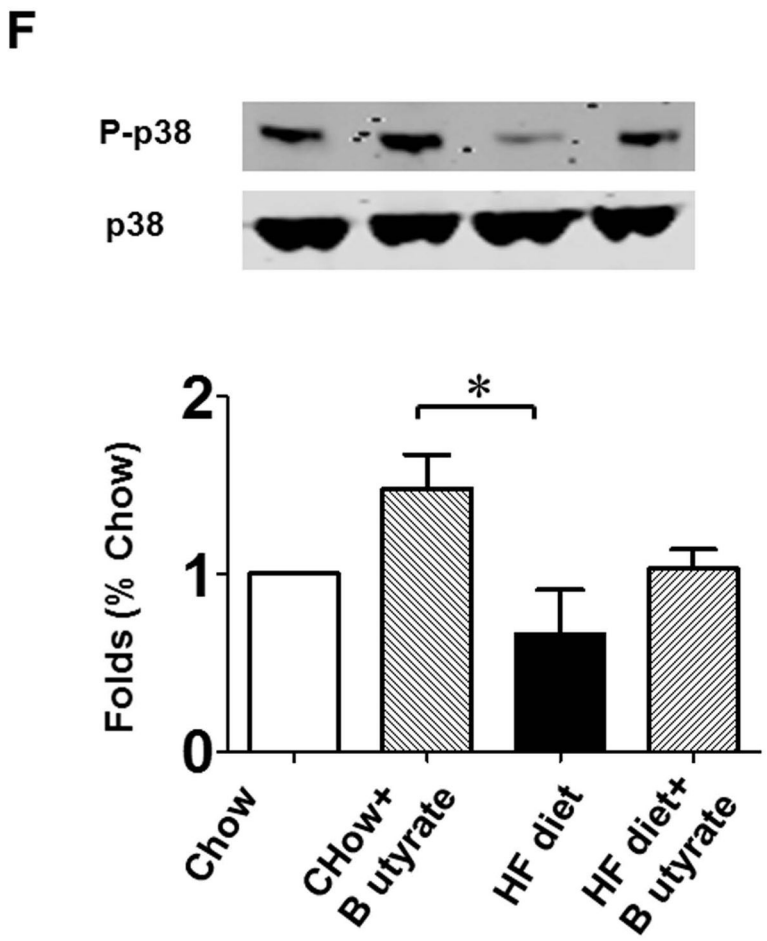

G

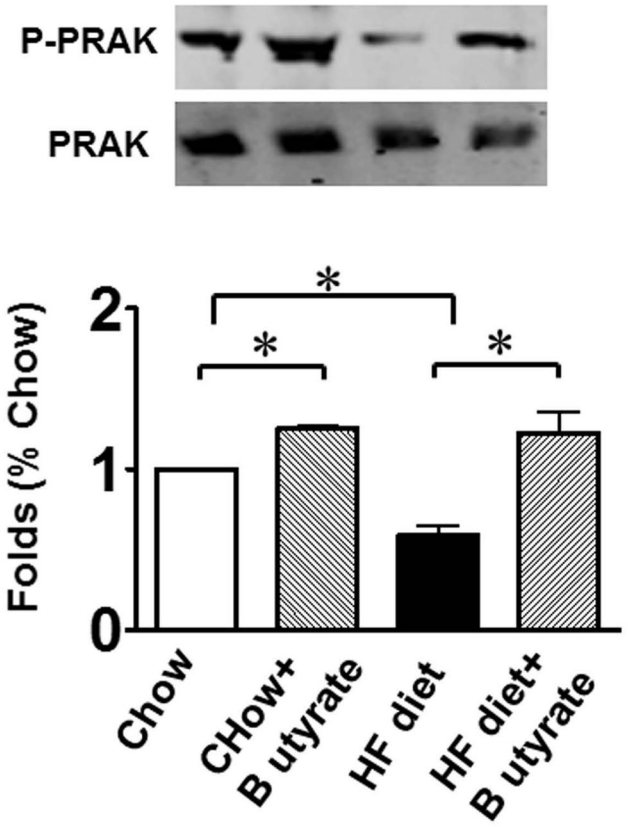

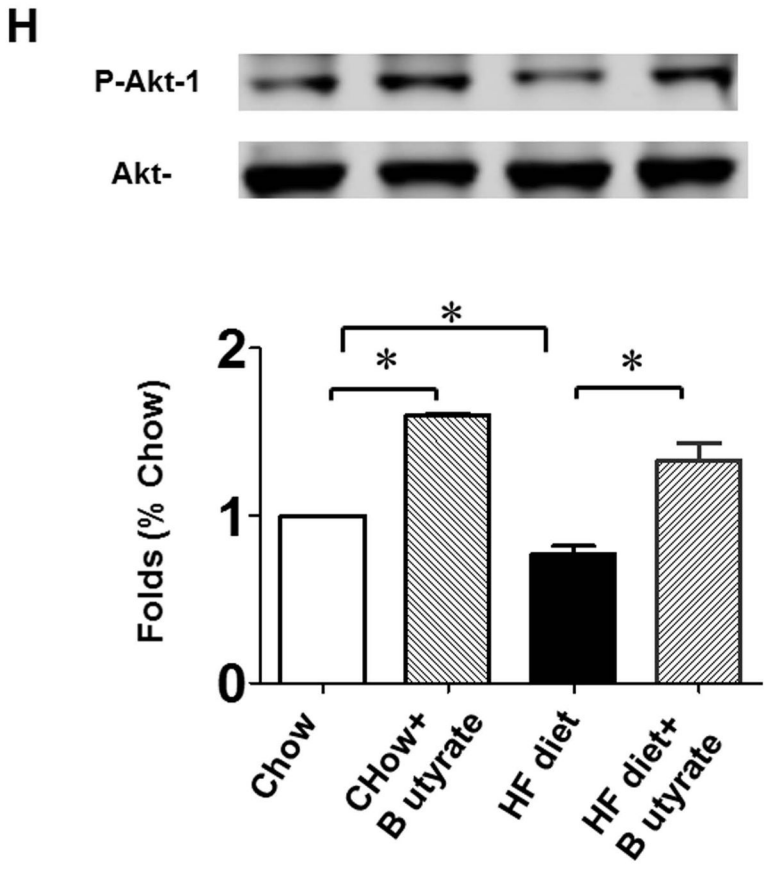

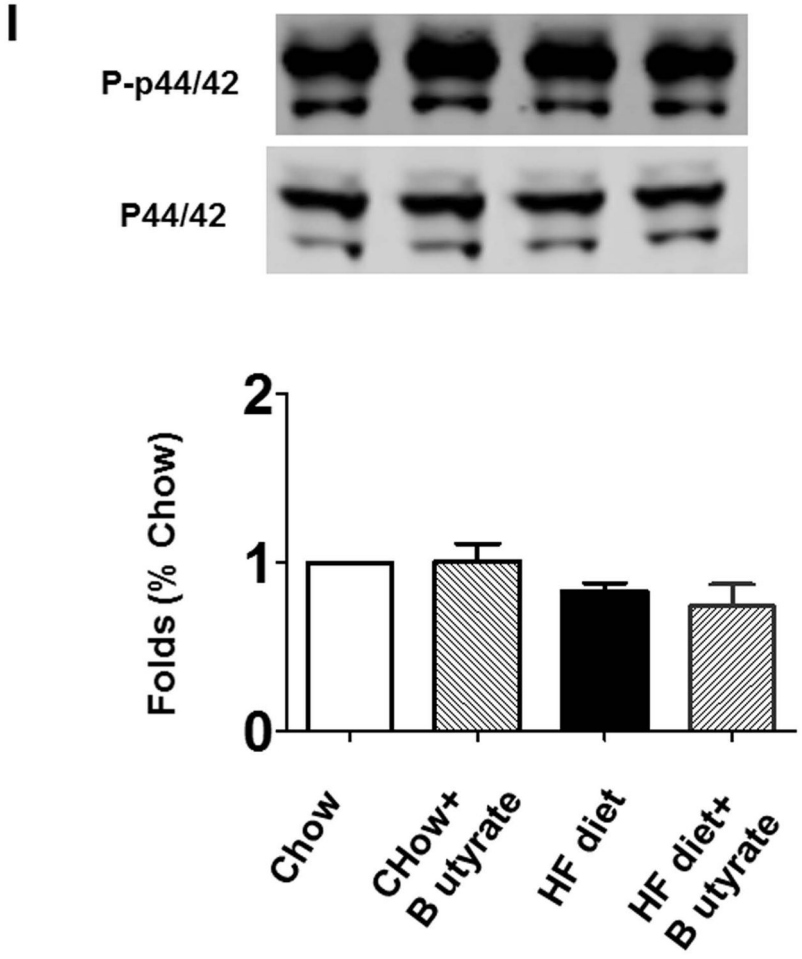

Figure 7. Sodium butyrate treatment promotes angiogenesis in HFD-induced diabetic heart

A: Representative images of CD31 staining. **B**: Quantitative analysis of angiogenesis. Results were indicated by the number of CD31-positive cells per mm^2. Values are shown as mean ± SEM (n = 4–5 per group); * $p < 0.05$. Scale bar: 100μm.

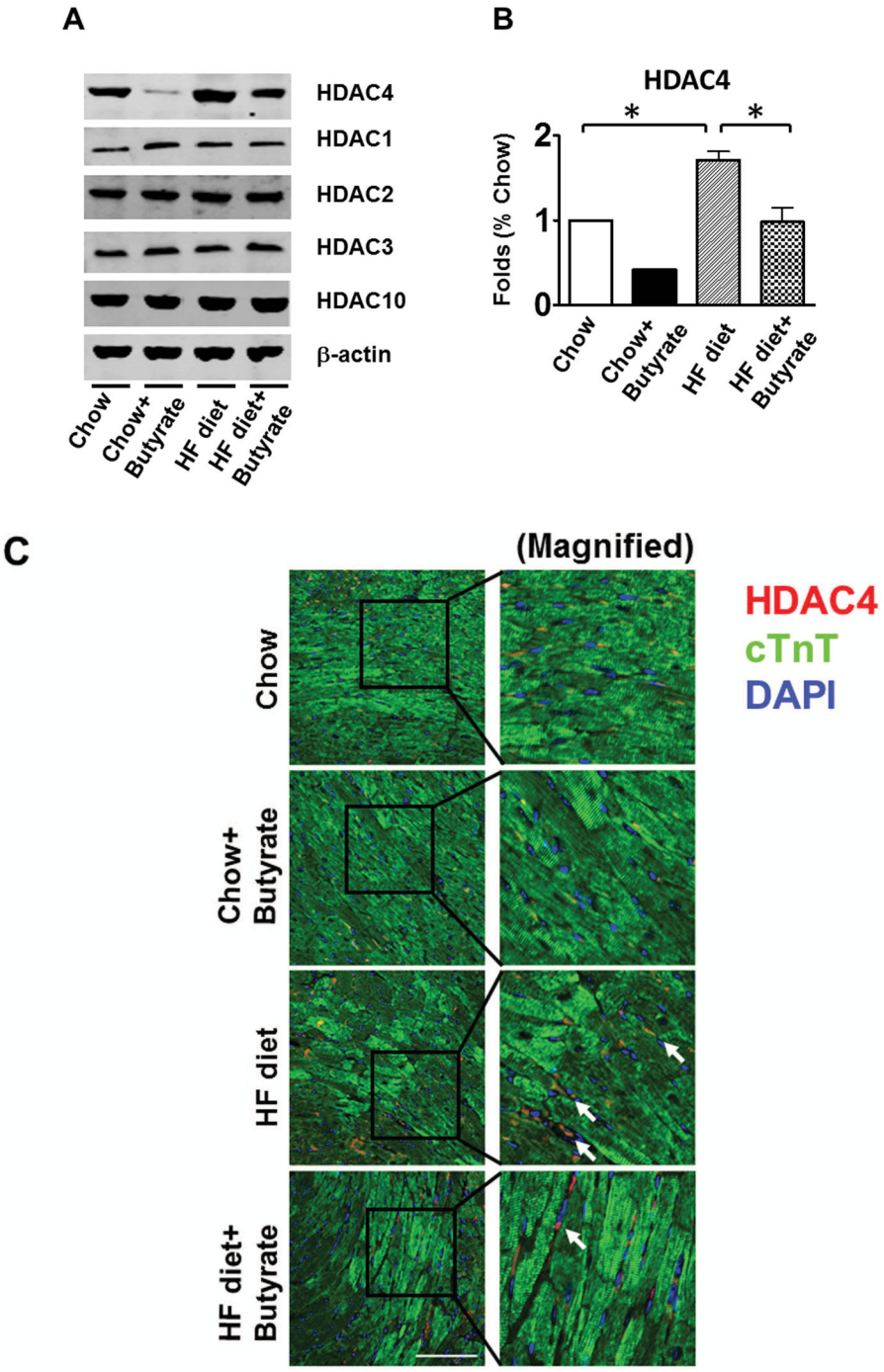

Figure 8. Sodium butyrate treatment induced alterations in signaling pathways in myocardium

Lysates from left ventricle of control and experimental mice were subject to western blotting using antibodies against HDAC 1, HDAC2, HDAC3, HDAC4, HDAC10 (**A); B**: The bar graph shows the densitometric scanning results (n=3 per group). * $p<0.05$. **C**: Immunostaining showing that HDAC4 was increased in myocardium exposed to HFD-fed heart. HDAC4 was shown in red; cardiomyocytes was shown in green (cTnT); Nuclei was shown in blue (DAPI); HFD increased HDAC4 positive staining. Scale bar=100um; **D**:

HDAC activity was measured in myocardium from different groups (n=3/per group), ***p<0.001. **E**: Western blot showing sodium butyrate enhanced MKK3 phosphorylation. The bar graph shows the densitometric scanning results (means ± SEM) (n=3 per group). * $p<0.05$, HFD: High fat diet. **F**: Western blot showing that sodium butyrate enhanced p38 phosphorylation (means ± SEM) (n=3 per group). * $p<0.05$ vs HFD: High fat diet. **G**: Western blot showing sodium butyrate enhanced PRAK phosphorylation (means ± SEM) (n=3 per group). * $p<0.05$. **H**: Western blot showing sodium butyrate enhanced Akt-1 phosphorylation (means ± SEM) (n=3 per group). * $p<0.05$. **I**: Western blot showing sodium butyrate did not affect p44/42 phosphorylation (means ± SEM) (n=3 per group).

Table 1

The parameters of left ventricular internal dimension in systole (LVID;s) in the development of cardiac dysfunction in type II diabetes and obesity.

	Chow	Chow-NAB	HFD	HFD-NAB
Week	mean±SEM	mean±SEM	mean±SEM	mean±SEM
0	0.94±0.09	0.94±0.09	0.94±0.09	0.94±0.09
8	1.15±0.12	1.33±0.05	1.38±0.08	1.38±0.04
16	1.12±0.04	1.08±0.01	1.63±0.07****	1.38±0.02##
24	1.18±0.02	0.87±0.01	1.73±0.05****	1.00±0.08####

**** p<0.0001, Compared with chow food group

p<0.01, Compared with HFD group

p<0.0001, Compared with HFD group (n=4–5/per group)

HFD; High fat diet; NAB: sodium butyrate.

Table 2

The parameter of left ventricular internal dimension in diastole (LVID;d) in the development of cardiac dysfunction in type II diabetes and obesity.

	Chow	Chow-NAB	HFD	HFD-NAB
Week	mean±SEM	mean±SEM	mean±SEM	mean±SEM
0	2.66±0.08	2.66±0.08	2.66±0.08	2.66±0.12
8	2.96±0.06	3.25±0.08	2.7±0.08	3.02±0.10
16	3.16±0.11	2.875±0.10	2.85±0.17	2.9±0.08
24	2.82±0.08	2.87±0.06	3.575±0.07****	2.82±0.05####

**** p<0.0001, Compared with chow food group

p<0.0001, Compared with HFD group (n=4–5/per group)

HFD; High fat diet; NAB: sodium butyrate.

Table 3

The parameters of ejection fraction (EF) in the development of cardiac dysfunction in type II diabetes and obesity.

	Chow	Chow-NAB	HFD	HFD-NAB
Week	mean±SEM	mean±SEM	mean±SEM	mean±SEM
0	94.98±0.95	94.98±0.95	94.98±0.95	94.98±0.95
8	96.15±1.68	89.60±2.39	84.96±4.75	81.13±1.73
16	89.68±3.08	89.50±2.57	71.90±2.65 **	82.73±2.99
24	84.22±2.50	86.67±1.08	66.55±2.39 ****	85.12±0.97####

** p<0.01, Compared with chow food group

**** p<0.0001, Compared with chow food group

p<0.0001, Compared with HFD group (n=4–5/per group)

HFD; High fat diet; NAB: sodium butyrate.

Table 4

The parameters of fractional shortening (FS) in the development of cardiac dysfunction in type II diabetes and obesity.

	Chow	Chow-NAB	HFD	HFD-NAB
Week	mean±SEM	mean±SEM	mean±SEM	mean±SEM
0	64.66±2.62	64.66±2.62	64.66±2.62	64.66±2.62
8	67.96±1.62	69.25±5.41	57.10±2.83	55.08±3.64
16	65.84±1.82	62.43±2.39	50.93±2.65 *	54.48±4.39
24	60.60±2.36	59.83±3.45	40.10±1.43 ***	64.80±2.07####

* p<0.05, Compared with chow food group

*** p<0.001, Compared with chow food group

p<0.0001, Compared with HFD group (n=4–5/per group)

HFD; High fat diet; NAB: sodium butyrate.